Research Article

Jamel Bouslimi*, Ali A. Alkathiri, Abdulaziz N. Alharbi, Wasim Jamshed, Mohamed R. Eid*, and Mohamed Lamjed Bouazizi

Dynamics of convective slippery constraints on hybrid radiative Sutterby nanofluid flow by Galerkin finite element simulation

https://doi.org/10.1515/ntrev-2022-0070
received December 17, 2021; accepted February 16, 2022

Abstract: The heat transport and entropy formation of an unsteady Sutterby hybrid nanofluid (SBHNF) are investigated in this work. SBHNF's flowing and thermal transport properties are investigated by exposing the nanofluid to a slippery hot surface. This analysis includes the influences of solid-shaped nanoparticles, porous materials, radiative flux, and viscous dissipative flow. The Galerkin finite element technique (G-FEM) is used to find self-similar solutions to equations that are then transformed into ODEs using appropriate transformations. This research considers two diverse kinds of nano-solid-particles, copper (Cu) and graphene oxide (GO), using non-Newtonian engine-oil (EO) as the working fluid. In the flowing, energy, skin friction, Nusselt number, and entropy production, important findings for the various variables are visually depicted. The most notable finding of the analysis is that when SBHNF (GO–Cu/EO) is compared to a typical nanofluid (Cu–EO), the thermal transmission rate of SBHNF (GO–Cu/EO) gradually increases. Furthermore, heat transfer is greatest for spherical-shaped nanoparticles and lowest for lamina-shaped nanoparticles. The entropy in the model is increased when the size of the nanoparticles ϕ is increased. The comparable impact is noticed once the radiation flowing N_r and Deborah number λ increase.

Keywords: Sutterby hybrid nanofluid, entropy generation, viscous dissipation, finite element, shaped-factor

*** Corresponding author: Jamel Bouslimi,** Department of Physics, College of Science, Taif University, P.O. Box 11099, Taif 21944, Saudi Arabia, e-mail: jamelabouaysem@yahoo.fr
*** Corresponding author: Mohamed R. Eid,** Department of Mathematics, Faculty of Science, New Valley University, Al-Kharga, Al-Wadi Al-Gadid, 72511, Egypt; Department of Mathematics, Faculty of Science, Northern Border University, Arar, 1321, Saudi Arabia, e-mail: m_r_eid@yahoo.com
Ali A. Alkathiri, Abdulaziz N. Alharbi: Department of Physics, College of Science, Taif University, P.O. Box 11099, Taif 21944, Saudi Arabia
Wasim Jamshed: Department of Mathematics, Capital University of Science and Technology (CUST), Islamabad, 44000, Pakistan
Mohamed Lamjed Bouazizi: Department of Mechanical Engineering, College of Engineering, Prince Sattam bin Abdulaziz University, Alkharj 16273, Saudi Arabia

Abbreviations

A	unsteadiness parameter
b	initial stretching rate
B_i	Biot number
B_r	Brinkman number
C_f	frictional force factor
C_p	specific heat (J kg^{-1} K^{-1})
E_G	dimensional entropy (J/K)
E	column vectors of order
E_c	Eckert number
h	heat transport factor
κ	thermal conductivity (W m^{-1} K^{-1})
k_0	thermal conductivity of the surface
k^*	absorbent factor
n	power-law index
N_r	radiation parameter
N_G	dimensionless entropy generation
Nu_x	local Nusselt number
P_r	Prandtl number (ν/α)
q_r	radiative heat flux
q_w	wall heat flux
Q	heat source
R_e	Reynolds number
S	suction/injection parameter
v_1, v_2	velocity component (m s^{-1})
U_w	velocity of the stretching sheet
V_w	vertical velocity
x, y	dimensional space coordinates (m)

Greek symbols

¥	fluid temperature
ξ	effective extending rate
$¥_w$	temperature at wall
$¥_\infty$	ambient temperature
ϕ	size of nanomolecules
ρ	density (kg m^{-3})
Ω	dimensionless temperature gradient
λ	Deborah number
σ^*	Stefan–Boltzmann constant
ψ	stream function
χ	similarity variable
θ	dimensionless temperature
Λ	velocity slip parameter
μ	dynamic viscosity (kg m^{-1} s^{-1})
ν	kinematic viscosity (m^2 s^{-1})
α	thermal diffusivity (m^2 s^{-1})

Subscripts

f, gf	base fluid
0	surface
p, p_1, p_2	nanoparticles
nf	nanofluid
hnf	hybrid nanofluid
s	particles
Cu	copper nanoparticles
GO	graphene oxide particles

1 Introduction

Nanofluid which has unusual characteristics and is well-known as the suspending colloidal fluid with metallic or nonmetallic nanosolid-particles was studied and discussed by several investigators. Buongiorno [1] said the absolute swiftness of the nanoparticles can be regarded as the total velocities of basefluid and the relative velocity. Seven slip processes were then analyzed: inertia, Brownian, thermophoretic diffusivity, diffusio-phoresis, Magnus impact, drainage of fluids, and gravitational change. Then, he announced that the Brownian and thermophoretic diffusions can play an imperative role in the non-attendance of turbulent impacts. Increased thermal conduction of conventional thermal transmission fluids, for example, H_2O, ethylene-glycol, and mineral oil, is achieved when nanoparticles are applied to a basic fluid. Nanofluids can thus be used for electrical cooling, cooling engines, solar water heating, nuclear reactor, oscillating heat tubing, and as transmission fluids for heat transmission [2]. Garoosi *et al.* [3] have studied numerically the nanofluids flowing in which using Buongiorno's model. Eiamsa-ard *et al.* [4] surveyed the improvement in heat transport of TiO_2–H_2O nanofluid into a heat exchanger tube fitted with superlative double-twisted strips. In different physical situations, recent additions are provided for the treatment of nanofluid with heat and mass transport [5–7].

Accurate simulation of nanofluid flowing with the macroscopic model is a prerequisite to building nanofluid-operating equipment [8]. Researchers have generally analyzed individual and two-phase macroscopic models. Provided that the relative speeds of nanoparticle and normal fluid are insignificant, the homogeneity monotonic model may be regarded as a single spectrum with its efficiencies. A homogeneous single-phase model has been used by Maiga *et al.* [9] for investigating forced convective flow of Al_2O_3–H_2O and Al_2O_3–EG nanoliquids in a homogeneously heated tube at completely established laminar and turbulent flowing schemes. Temperature-dependent characteristics for the convection of nano-fluid models have been shown to predict that those heat transfer improvements are greater than that of nanofluid-dependent model used by Palm *et al.* [10]. Xuan and Roetzel [11] have suggested the dispersion approach for nanofluids. Heris *et al.* [12] used a dispersive model for the simulation of laminar nanofluid convection in a rotating duct. Mokmeli and Avval [13] utilized both homogeneity monotonic and dispersive schemes for the study of convection nanofluid heat transport. When comparing numerical findings with experimental values, the dispersive model has been seen to be more correct [8]. A recent survey on single phase nanofluid flows is presented in refs. [14–16].

The trend in the numerical investigations of heat transport of nanoliquid is to consider it to be a Newtonian fluid; however, it is well documented that numerous nanofluids display a non-Newtonian behavior so it is important to consider it. Consequently, in this analysis, we take account of the significance of non-Newtonian liquid as a Sutterby liquid. Fluid model in the type of Sutterby explains the flux of pseudoplastic behavior. Non-Newtonian Sutterby fluid has been many uses, including those used to spin the fluid in the full process of drilling operations. These liquids are too utilized in fabricated lubricant processing. Refs [17–29] provide more detailed information.

The Sutterby fluid model exhibits highly refined polymer solutions and is one of the non-Newton-based liquids

used to analyze the rheological properties of various materials [30]. We are using the transition process to get the ODE system indirect. This program is solved numerically with a built-in shooting method. The leading values of the different parameters involved in speed, temperature, and concentration are defined. Speed, concentration, and temperature are calculated by numbers. The results obtained show that the speed is reduced by the parameter of the objects. Temperature and concentricity are augmented by the parameter [31]. The study of the behavior of non-Newtonian nanofluids is complex and difficult because of the indirect relationship between stress and stress level, and this is because many of the things that happen in the real world are not real and are not the same. It is very easy to solve a line problem but finding solutions to indirect problems is still very difficult. However, the results obtained by numerical methods give unstable points when sorted; otherwise, gaining a complete understanding of the indirect problem is also difficult. If an indirect problem involves unity or has many solutions this adds to the complexity of the numbers. Although numerical and mathematical methods for solving indirect problems are limited, they also have their advantages. Therefore, we cannot ignore any of these two methods, but it is usually fun to solve an indirect problem through analysis. In addition, perforated media is used to transport and conserve energy in many industrial systems, such as heat pipes, solid matrix heat exchangers, electric cooling, and chemical reactors [32]. Various solutions were reported by Hashim and Hamid [33] on Williamson nanofluid flow about suction variable in the current decade. There have been more recent debates [34–36] in regards to non-Newtonian nanofluids. Refs [37–48] provide recent information that considers nanofluids with flowing and heat transmission in a variety of physical descriptions.

Hybrid nanofluids were introduced by Suresh *et al.* [49] to extra improve the optimistic characteristics of nanoliquids. Hybrid nanofluids are built by the combination of two different kinds of nanosolid-particles. Recent research in the area of nanofluids has focused on hybrid nanofluid thermal systems. The effect of various kinds of nanoparticles, nanoparticle sizes, the volume of nanosolid-particles in the basis fluid, and thermophysical characteristics of nanofluids is nonetheless crucial. The three-dimensional flux of $Cu–Al_2O_3/H_2O$ hybrid nanofluid using the RK-Fehlberg integrated process is analyzed by Devi and Devi [50]. This is caused by Lorentz's force by the unidirectional linear expansion of the plate. The findings showed that the $Cu–Al_2O_3/H_2O$ hybrid nanofluid heat exchange rate is higher than that of $Cu–H_2O$ nanofluid. Afrand *et al.* [51] examinated the influence on the rheology conduct of magnetite hybrid nanofluid-silver/ethylene glycol (Fe_3O_4–Ag/EG) of temperature distribution and nanoparticulate concentration. Hayat and Nadeem [52] took the hybrid Brinkman nanoliquid 3D flow, for an assessment of heat transfer characteristics on a linear extending and circular surface with radiative and homogeneity (heterogeneity) reactive flowing of CuO/H_2O and $Ag–CuO/H_2O$. Ghadikolaei *et al.* [53] scrutinized the thermo-physical characteristics of magnetohydrodynamics (MHD) mixture $TiO_2–Cu/H_2O$ nanofluid with common geometrical shapes factor for nanoparticles. Hussain *et al.* [54] considered a hybrid nanofluid containing $Al_2O_3–Cu/H_2O$ flowing into an open cavity with an adiabatic quadrangular obstruction within the hollow. For numerical solution, the finite element method was utilized and the influences of various potential factors on hybrid nanofluid were addressed. Information on mixture nanoliquid flowing and heat transmission properties can be found in refs [55–59].

Recently, the thermodynamics second-law was employed [60] in order to minimize entropy production to find the optimum engineering scheme. The level of irresponsibilities accumulating during a process has been decided with entropy generation [61]. This can be used to test the efficiency of engineering devices with entropy analysis [62]. For example, Oztop and Salem [63] carried out an analysis of the entropy production for free and mixed convective heat transport models. A final volume approach was taken by Shahzad *et al.* [64] to examine wavy channel entropy and thermohydraulic efficiency with three-corrugation outlines, which are trapezoidal, sinusoidal, and triangular. Iron salt, tannin, and graphic oxide were assembled into $GO–Fe_3O_4$ hybrid nanofluid by Mehrali *et al.* [65] due to the stability and abundance. The overall thermal conductance of the system can be increased by 11% with the usage of hybrid solid nanoparticles. Under the effect of a magnetic field, the efficacy of heat transfer of $GO–Fe_3O_4$ mixed nanofluid enhances, while entropy is decreased with graphene usage instead of purified H_2O by 41%. Using a hot stretched plate, Shahzad *et al.* [66] made an analysis on chemical reactions and entropy of the 2nd-grade nanofluid under the effect of nonlinear heat radioactivities and MHD. Increment in Reynolds, Brinkmann, and Hartmann numbers results in system entropy elevating, while reduction is observed for higher temperature. Similar analyses were conducted in refs [67–71] for entropy production of nanofluid with the expandable surfaces using diverse geometry.

The finite element technique is commonly used in mathematics and engineering models to numerically solve differential equations. Other applications include sophisticated geometry testing and different forms of

material modeling. Khan *et al.* [72] developed a design-based model to investigate heat increase and thermal management in a separate lid-driven square cavity. They got numerical results using the Galerkin finite element approach (G-FEM). Mourad *et al.* [73] investigated uniform MHD free convection and heat transmission in a penetrable cavity using a hybrid Fe_3O_4-MWCNT/water nanofluid filled inner elliptic cylinder. To validate the governing equations, they employed the G-FEM. Rana *et al.* [74] presented an investigation on the electromagnetism aspect of nanofluid on an expandable cylinder under the suspension influence of gyrotactic algae using the Cattaneo–Christov mass and heat flux concept. They used the finite element approach to acquire the mathematical conclusions of the model's governing equations. Shah *et al.* [75] investigated the magnetized non-Darcy flow of free convective hybrid nanofluid on a penetrable cylinder using a stable and ambient magnetic field as well as a constant heat source. To numerically resolve the governing set of equations, the control volume finite element approach was used. Nasrin *et al.* [76] probed the heat transmission behavior of mixture nanoliquids using sinusoidal and lid-driven cavities with trapezoidal shapes. They used the finite element approach to solve the controlling set of partial differential equations regulating fluid temperature and velocity.

Studies on entropy production of SBHNF are infrequent, and none of the papers available addressed the impacts of a penetrable material, viscous dissipation, and radiation flux, shaped-factor *via* the extended sheet utilizing the nanoliquid Tiwari–Das scheme in detail [77]. The fluid, swiftness, and temperature in Tiwari-Das (monotonic model) are equivalent. The advantages of the single-phase approach are that the slip processes are ignored so that the model is simpler and numerically easy to solve. But the downside of the approach is that the numerical effects of certain situations vary from the results of experiments. Concentrations range from 3 to 20% in this model volume of nanoparticles. The effects of Cu–EO, GO–EO hybrid, and standard nanofluid were only approximated by numerical findings. Therefore, the present investigation focuses on the powerful liquid feature effects and entropy in a numbered system based on the Keller-box process (KBM) of SBHNF in a boundary-layer in order to bridge a gap.

The structure of the current article is as follows: governing mathematical equations are given in Section 2. Solution to the problem is established in Section 3. Galerkin finite element method employed during the numbering procedure is explained in Section 4. Section 5 tells about the validation of the code. In Section 6, we analyzed the development of entropy. Section 7 summarizes the findings as well as the debate. Outcomes along with future guidelines are provided in Section 8.

2 Flow model formulations

The mathematical flow equations show the moved horizontal plate with the irregular expanding velocity [78]:

$$U_w(x, t) = \frac{bx}{1 - \xi t}, \tag{2.1}$$

where b is an original expanding rate. $¥_w(x, t) = ¥_\infty + \frac{b^* x}{1 - \xi t}$ is isolated surface temperature, for appropriateness, it is considered as constant at $x = 0$. Here b^*, $¥_w$, and $¥_\infty$ represent the rate of temperature variation, the temperature of the surface, and temperature of surroundings, respectively. According to the assumptions, the plate is slippery and temperature variation is subjected to the surface. The hybrid nanofluid is formulated at first with the addition of Cu solid nanoparticles in EO as basefluid at a fractional size (ϕ_R) and it is constant at 0.09 throughout the investigation. Graphene oxide GO nanomolecules have been expanded in the mixture to achieve a hybrid nanofluid at the concentricity volume (ϕ_H).

2.1 Suppositions and terms of model

Following are the principles along with restrictions applicable to the flowing model:

- two-dimensional laminar unsteady flowing,
- boundary-layer estimates,
- Tiwari and Das (single-phase) technique,
- non-Newtonian SBHNF,
- porous medium,
- thermal radiation flux,
- viscous dissipation flow,
- shape-factor of nanomolecules,
- copper (Cu) and graphene oxide (GO) nanoparticles,
- engine-oil (EO) as the base fluid,
- porous elongated surface,
- slippery as well as convection boundary restrictions.

2.2 Sutterby fluid stress-tensor

In Sutterby model, the stress-tensor is defined as

$$T = -pI + S. \tag{2.2}$$

where p and I denote pressure and identity-tensor, respectively, whereas S denotes an additional stress-tensor.

$$S = \mu_0 \left[\frac{\sinh^{-1}(E\dot{\gamma})}{E\dot{\gamma}} \right]^{\varsigma} A_1, \tag{2.3}$$

where μ_0 and E denote zero-shear rate viscosity and material time-constant, respectively. Underneath are the mathematical equations for the second invariant strain tensor $\dot{\gamma}$ and the first order Rivlin–Ericksen tensor A_1.

$$\dot{\gamma} = \sqrt{\frac{\mathrm{tr}(A_1)^2}{2}}, \tag{2.4}$$

and

$$A_1 = (\mathrm{grad}\ V) + (\mathrm{grad}\ V)^T. \tag{2.5}$$

In the case of $\varsigma = 0$, the fluid is equivalent a Newtonian fluid, while at $\varsigma > 0$ it is pseudoplastic (shear-thinning) fluid, and $\varsigma < 0$ is dilatant (shear-thickening) fluid.

2.3 Geometric model

Figure 1 depicts the geometrical flow concept.

Figure 1 depicts the diagram of the flowing model. The flowing in this scheme is caused by the unidirectional extending of the surface. The flow slippery phenomenon occurs at the plate, and thermal jumping is used to transmit heat from the lamina to the liquid.

2.4 Model equations

The constituent flow formulas [79] of viscid SBHNF that have been adeptly modified with porous material, thermal radiative, and viscous dissipative flow under the accustomed boundary-layer approximation are

$$\frac{\partial v_1}{\partial x} + \frac{\partial v_2}{\partial y} = 0, \tag{2.6}$$

$$\frac{\partial v_1}{\partial t} + v_1\frac{\partial v_1}{\partial x} + v_2\frac{\partial v_1}{\partial y} = \frac{\mu_{\mathrm{hnf}}}{\rho_{\mathrm{hnf}}}\frac{1}{2}\frac{\partial^2 v_1}{\partial y^2}\left(1 - \frac{nb^2}{2}\left(\frac{\partial v_1}{\partial y}\right)^2\right) - \frac{\mu_{\mathrm{hnf}}}{\rho_{\mathrm{hnf}}k}v_1, \tag{2.7}$$

$$\frac{\partial ¥}{\partial t} + v_1\frac{\partial ¥}{\partial x} + v_2\frac{\partial ¥}{\partial y} = \frac{k_{\mathrm{hnf}}}{(\rho C_p)_{\mathrm{hnf}}}\left(\frac{\partial^2 ¥}{\partial y^2}\right) - \frac{1}{(\rho C_{\mathrm{p}})_{\mathrm{hnf}}}\left(\frac{\partial q_{\mathrm{r}}}{\partial y}\right) + \frac{1}{(\rho C_{\mathrm{p}})_{\mathrm{hnf}}}Q(¥ - ¥_\infty) + \frac{\mu_{\mathrm{hnf}}}{(\rho C_{\mathrm{p}})_{\mathrm{hnf}}}\left(\frac{\partial v_1}{\partial y}\right)^2. \tag{2.8}$$

Aziz *et al.* [58] gave the related boundary constraints:

$$v_1(x, 0) = U_{\mathrm{w}} + N_{\mathrm{w}}\left(\frac{\partial v_1}{\partial y}\right),\ v_2(x, 0) = V_{\mathrm{w}}, \quad -k_0\left(\frac{\partial ¥}{\partial y}\right) = h_{\mathrm{f}}(¥_{\mathrm{w}} - ¥), \tag{2.9}$$

$$v_1 \to 0,\ ¥ \to ¥_\infty \ \text{ as } \ y \to \infty. \tag{2.10}$$

Vector of flow velocity is defined as $\overleftarrow{v} = [v_1(x, y, t), v_2(x, y, t), 0]$. Time is represented by t, and ¥ presents the temperature of the fluid. Q is the heat source. N_{w} is the slip length, V_{w} is the porosity of the extending plate, while k symbolizes the porousness of the material.

2.5 Physical thermal characteristics of SBNF

Nanomolecules spread in EO induce modified thermophysical properties. The equations of Table 1 synopsizes SBNF variables of the material [80,81].

The nanoparticles volume factor ϕ is seen in Table 1. The standard fluid's dynamical viscidity, density, working heat capacity, and thermal and electrical conductivities are

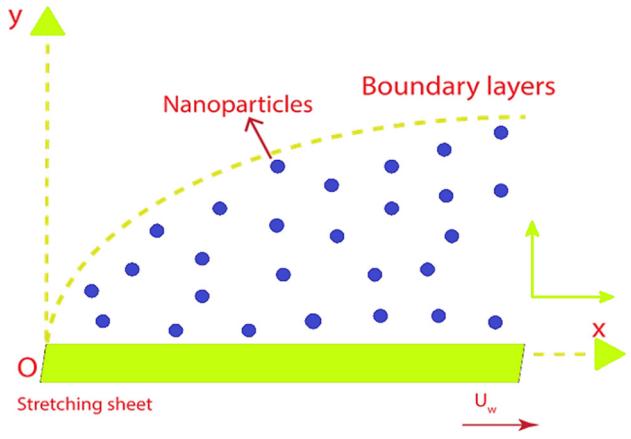

Figure 1: Scheme of the flow paradigm.

Table 1: Thermo-physical features for nanoliquids

Features	Nanoliquid
Dynamical viscidness (μ)	$\mu_{\mathrm{nf}} = \mu_{\mathrm{f}}(1-\phi)^{-2.5}$
Density (ρ)	$\rho_{\mathrm{nf}} = (1-\phi)\rho_{\mathrm{f}} - \phi\rho_{\mathrm{s}}$
Heat capacity (ρC_{p})	$(\rho C_{\mathrm{p}})_{\mathrm{nf}} = (1-\phi)(\rho C_{\mathrm{p}})_{\mathrm{f}} - \phi(\rho C_{\mathrm{p}})_{\mathrm{s}}$
Thermal conductivity (κ)	$\frac{\kappa_{\mathrm{nf}}}{\kappa_{\mathrm{f}}} = \left[\frac{(\kappa_{\mathrm{s}} + (m-1)\kappa_{\mathrm{f}}) - (m-1)\phi(\kappa_{\mathrm{f}} - \kappa_{\mathrm{s}})}{(\kappa_{\mathrm{s}} + (m-1)\kappa_{\mathrm{f}}) + \phi(\kappa_{\mathrm{f}} - \kappa_{\mathrm{s}})}\right]$

represented by μ_f, ρ_f, $(C_p)_f$ and κ_f, respectively. The density, heat capacity, and thermal conductivity of the nanoparticle are represented by ρ_s, $(C_p)_s$, and κ_s, respectively.

2.6 Thermo-physical characteristics of SBHNF

The suspension of two unique kinds of nanomolecules inside the basic fluid is the main premise of hybrid nanofluids [82]. This boosts the heat transfer capability of conventional liquids and makes them a better heat interpreter than nanofluids. Table 2 demonstrates the content of SBHNF variables [57,59].

Dynamic viscidity of mixture nanofluid, density, specific heat capacity, and thermal conductivity are all listed in Table 2 as μ_{hnf}, ρ_{hnf}, $\rho(C_p)_{hnf}$, and κ_{hnf}. ϕ represents the volumetric coefficient of solid nanomolecules in a mono nanofluid. For the mixed nanofluid, $\phi_{hnf} = \phi_R + \phi_H$ is the coefficient of hybrid nanoparticles. The dynamical viscidity, density, specific heat capacity, and thermal conductivity of the basefluid are represented by μ_f, ρ_f, $(C_p)_f$, κ_f, and σ_f. The densities, specific heat capacitances, and thermal conductances of the nanomolecules are represented by ρ_{p_1}, ρ_{p_2}, $(C_p)_{p_1}$, $(C_p)_{p_2}$, κ_{p_1}, and κ_{p_2}, where the subscripts p_1 and p_2 represents Cu and GO nanomolecules, respectively.

The nanomolecules' shaped-factor defines the size of numerous nanomolecules. The empirical particle form factors are sphere = 3, hexahedron = 3.7221, tetrahedron = 4.0613, column = 6.3698, and lamina = 16.1576 [83].

2.7 Nanosolid-particles and basefluid lineaments

In Table 3 [84–86] of analysis, substantial features of the primary fluid of the engine oil are described.

Table 3: Fabricated materials' thermo-physical attributes

Thermo-physical	ρ (kg/m^3)	c_p (J/kgK)	k (W/mK)
Copper (Cu)	8,933	385.0	401.00
Engine oil (EO)	884	1,910	0.144
Graphene oxide (GO)	1,800	717	5,000

2.8 Rosseland approximation

Due to the thicker non-Newtonian SBHNF, only a shortened distance can be covered by the radiative flow. So, the equation for Rosseland radiative flux given by Brewster [87] is applied in formula (2.8).

$$q_r = -\frac{4\sigma^*}{3k^*}\frac{\partial T^4}{\partial y}, \tag{2.11}$$

where σ^* signifies Stefan–Boltzmann constant and k^* symbolizes the rate.

3 Nondimensional transformed system

According to similarity transformation converting the controlling partial differential equations into ordinary differential equations (ODEs), equations (2.7) and (2.8) are boundary-value problem. Stream function ψ is specified as:

$$v_1 = \frac{\partial \psi}{\partial y},\ v_2 = -\frac{\partial \psi}{\partial x}. \tag{3.1}$$

The next specified similarity quantities are applied

$$\chi(x,y) = \sqrt{\frac{b}{\nu_f(1-\xi t)}}\,y,$$
$$\psi(x,y) = \sqrt{\frac{\nu_f b}{(1-\xi t)}}\,x f(\chi),\ \theta(\chi) = \frac{¥ - ¥_\infty}{¥_w - ¥_\infty}, \tag{3.2}$$

Table 2 Thermo-: physical properties of hybrid nanofluids

Features	Hybrid nanofluid
Viscosity (μ)	$\mu_{hnf} = \mu_f(1-\phi_R)^{-2.5}(1-\phi_H)^{-2.5}$
Density (ρ)	$\rho_{hnf} = [(1-\phi_H)\{(1-\phi_R)\rho_f + \phi_R\rho_{p_1}\}] + \phi_H\rho_{p_2}$
Heat capacity (ρC_p)	$(\rho C_p)_{hnf} = [(1-\phi_H)\{(1-\phi_R)(\rho C_p)_f + \phi_R(\rho C_p)_{p_1}\}] + \phi_z(\rho C_p)_{p_2}$
Thermal conductivity (κ)	$\frac{\kappa_{hnf}}{\kappa_{gf}} = \left[\frac{(\kappa_{p_2}+(m-1)\kappa_{gf})-(m-1)\phi_H(\kappa_{gf}-\kappa_{p_2})}{(\kappa_{p_2}+(m-1)\kappa_{gf})+\phi_H(\kappa_{gf}-\kappa_{p_2})}\right]\frac{\kappa_{gf}}{\kappa_f} = \left[\frac{(\kappa_{p_1}+(m-1)\kappa_f)-(m-1)\phi_R(\kappa_f-\kappa_{p_1})}{(\kappa_{p_1}+(m-1)\kappa_f)+\phi_R(\kappa_f-\kappa_{p_1})}\right]$

in equations (2.7) and (2.8). We get

$$f''' + 2\phi_a\phi_b\left(ff'' - f'^2 + A\left(f' + \frac{\chi}{2}f''\right)\right) - \frac{n}{2}\lambda R_e f''^2 f''' - 2Kf' = 0, \tag{3.3}$$

$$\theta''\left(1 + \frac{1}{\phi_d}P_r N_r\right) + P_r\frac{\phi_c}{\phi_d}\left[f\theta' - f'\theta + -A\left(\theta + \frac{\chi}{2}\theta'\right)\theta\frac{Q}{\phi_c} + \frac{E_c}{\phi_a\phi_c}f''^2\right] = 0, \tag{3.4}$$

with

$$\left.\begin{aligned} &f(0) = S,\ f'(0) = 1 + \Lambda f''(0),\\ &\theta'(0) = -B_i(1 - \theta(0))\\ &f'(\chi) \to 0,\ \theta(\chi) \to 0, \quad \text{as}\ \ \chi \to \infty \end{aligned}\right\}, \tag{3.5}$$

where χ and θ signify the similarity variable and nondimensional temperature, respectively. In equations (3.3)–(3.4), the consecutive thermo-physical structures ϕ_a, ϕ_b, ϕ_c, and ϕ_d for SBHNF are specified as

$$\phi_a = (1 - \phi_1)^{2.5}(1 - \phi_2)^{2.5},$$
$$\phi_b = (1 - \phi_2)\left[(1 - \phi_1) + \phi_1\frac{\rho_{p_1}}{\rho_f}\right] + \phi_2\frac{\rho_{p_2}}{\rho_f}, \tag{3.6}$$

$$\phi_c = (1 - \phi_2)\left\{(1 - \phi_1) + \phi_1\frac{(\rho C_p)_{p_1}}{(\rho C_p)_f}\right\} + \phi_2\frac{(\rho C_p)_{p_2}}{(\rho C_p)_f}, \tag{3.7}$$

$$\phi_d = \left[\frac{(\kappa_{p_2} + (m-1)\kappa_{nf}) - (m-1)\phi_2(\kappa_{nf} - \kappa_{p_2})}{(\kappa_{p_2} + (m-1)\kappa_{nf}) + \phi_2(\kappa_{nf} - \kappa_{p_2})}\right] \times \left[\frac{(\kappa_{p_1} + (m-1)\kappa_f) + \phi_1(\kappa_f - \kappa_{p_1})}{(\kappa_{p_1} + (m-1)\kappa_f) - (m-1)\phi_1(\kappa_f - \kappa_{p_1})}\right]. \tag{3.8}$$

It is noted that equation (2.8) is satisfied directly. In all formulas, $'$ symbols differentiate w.r.t χ. $A = \frac{\xi}{b}$, $\lambda = B^2b^2$, and $K = \frac{\nu_f(1-\xi t)}{bk}$, respectively, represent unsteadiness parameter, Deborah number, and porousness of material. $P_r = \frac{\nu_f}{\alpha_f}$ is the Prandtl amount. Thermal diffusivity parameter, thermal radiative flow, and mass transport are specified as $\alpha_f = \frac{\kappa_f}{(\rho C_p)_f}$, $N_r = \frac{16}{3}\frac{\sigma^* ¥_\infty^3}{\kappa^*\nu_f(\rho C_p)_f}$, and $S = -V_w\sqrt{\frac{1-\xi t}{\nu_f b}}$, respectively. $\Lambda = \sqrt{\frac{b}{\nu_f(1-\xi t)}}N_w$ is the slippery velocity parameter. $E_c = \frac{U_w^2}{(C_p)_f(T_w - T_\infty)}$ and $B_i = \frac{h_f}{k_0}\sqrt{\frac{\nu_f(1-\xi t)}{b}}$ are the Eckert number and Biot number, respectively. Similarity parameter (ξ) and time (t) are the parameters on which other variables depend. Hence, a non-similar solution for the model is obtained by determining the final results for locally related parameters.

3.1 Drag force and Nusselt number

The combination of drag force (C_f) and Nusselt number (Nu_x) are interesting physical quantities that can control the fluid flow and are specified as [79]

$$C_f = \frac{\tau_w}{\rho_f U_w^2},\ Nu_x = \frac{xq_w}{k_f(¥_w - ¥_\infty)}, \tag{3.9}$$

where τ_w and q_w are determined as

$$\tau_w = \mu_{hnf}\left(\left(\frac{\partial v_1}{\partial y}\right) + \frac{nB^2}{3}\left(\frac{\partial v_1}{\partial y}\right)^3\right)_{y=0},$$
$$q_w = -k_{hnf}\left(1 + \frac{16}{3}\frac{\sigma^* ¥_\infty^3}{\kappa^*\nu_f(\rho C_p)_f}\right)\left(\frac{\partial ¥}{\partial y}\right)_{y=0}. \tag{3.10}$$

The dimensionless transmutations (3.2) are implemented to obtain

$$C_f Re_x^{\frac{1}{2}} = \frac{1}{\phi_a}\left(f''(0) + \frac{n}{3}\lambda R_e f''(0)^3\right),$$
$$Nu_x Re_x^{-\frac{1}{2}} = -\frac{k_{hnf}}{k_f}(1 + N_r)\chi'(0),$$
$$[\chi_e, \chi_{e+1}] \tag{3.11}$$

where C_f represents the coefficient of drag force. $Re_x = \frac{u_w x}{\nu_f}$ is local R_e according to the elongated velocity $u_w(x)$.

4 G-FEM: A numerical method

Galerkin finite element technique [88] is used to do numerical computations for governing equations model. The following is a summary of FEM:

1) On the ordinary term $[\chi_e, \chi_{e+1}]$, the second order nonlinear terms are incorporated to give the powerless integral formulas with weighted remains.
2) To determine the term of stiffness parameters, powerless residual terms are replaced by finite element formulas.
3) To compute the rigidity factors, a normal term $[\chi_e, \chi_{e+1}]$ is used, which is then applied to the cluster technique of equations.
4) The collection of algebraic expressions obtained is linearized. To solve them further, an iterative technique is used with a 10^{-6} computational tolerance.
5) A calculational domain is generated by modifying the interval $[0, \infty)$ after identifying the greatest variable value

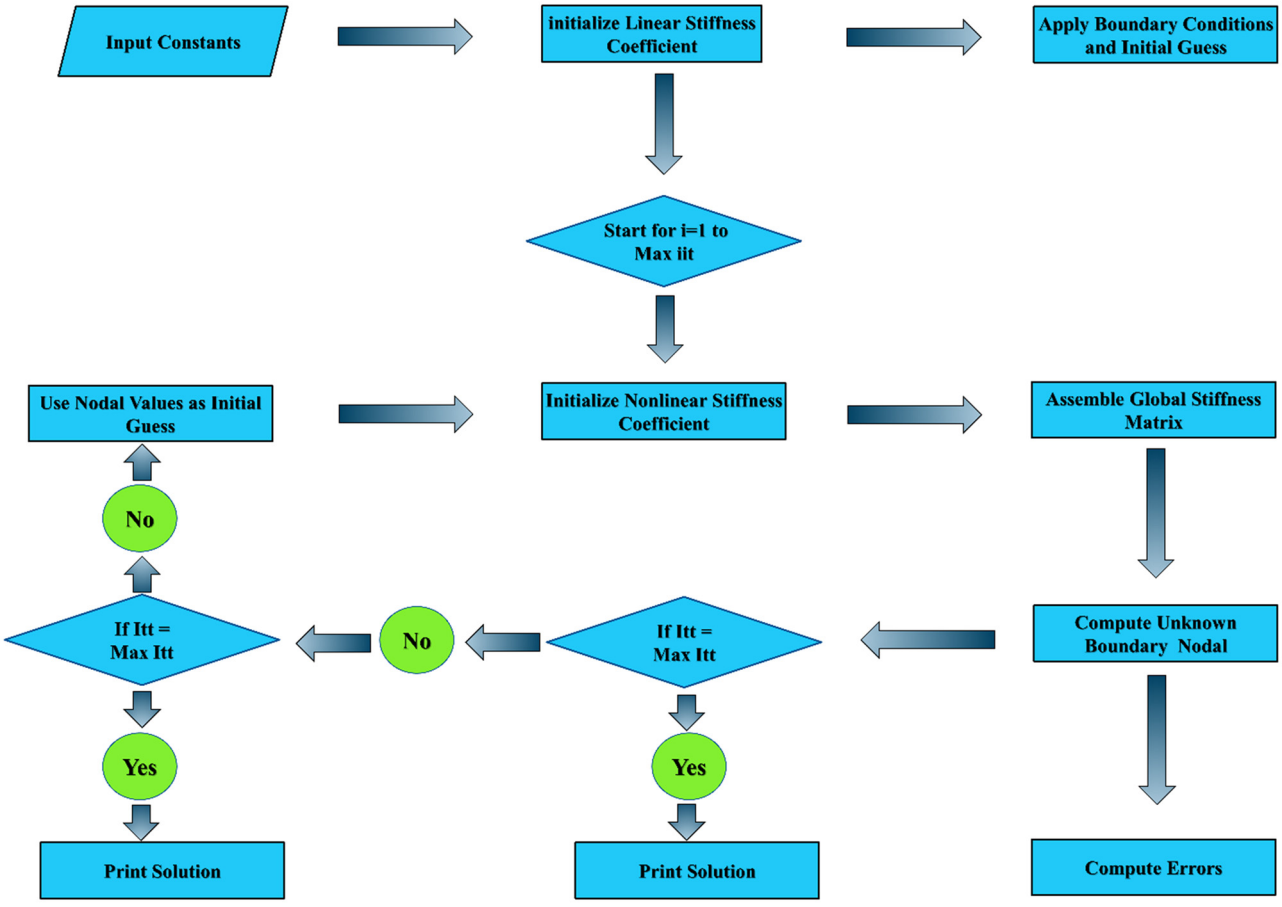

Figure 2: Flow chart of G-FEM.

6) Convergence is noticeable. To achieve decisive results, computations are done using a step size of $\Delta_\chi = 0.001$.

Figure 2 depicts the G-FEM flow diagram.

5 Code verification

Rate of heat transfer is measured, and the obtained results from the current method are compared with the results from the literature [89,90]. In this way, it can be seen that the method employed is valid. Comparison of some validities among a few analyses is presented in Table 4; however, results obtained during the current study are very accurate.

Unsteadiness of controlling equations was solved by Das *et al.* [89] with the help of RK-Fehlberg method. Jamshed *et al.* [90] used KBM to find the solution of the current model. KBM provides better and more accurate solutions compared with other methods.

Table 4: Comparing of $-\theta'(0)$ values with Pr, when $A = 0$, $\phi = 0$, $\phi_{\text{hnf}} = 0$, $Q = 0$, $E_c = 0$, $\Lambda = 0$, $N_r = 0$, $S = 0$, and $B_i \to 0$

P_r	Ref. [89]	Ref. [90]	Present
72×10^{-2}	0.80876122	0.80876181	0.80876181
1×10^{0}	1.00000000	1.00000000	1.00000000
3×10^{0}	1.92357431	1.92357420	1.92357420
7×10^{0}	3.07314679	3.07314651	3.07314651
10×10^{0}	3.72055436	3.72055429	3.72055429

6 Entropy analysis

The entropy of the system is generally increased by porous media. Entropy formation of the nanofluids is described as [90]:

$$E_G = \frac{k_{\text{hnf}}}{¥_\infty^2}\left\{\left(\frac{\partial ¥}{\partial y}\right)^2 + \frac{16}{3}\frac{\sigma^* ¥_\infty^3}{\kappa^* \nu_f (\rho C_p)_f}\left(\frac{\partial ¥}{\partial y}\right)^2\right\} + \frac{\mu_{\text{hnf}}}{¥_\infty}\left(\frac{\partial v_1}{\partial y}\right)^2 + \frac{\mu_{\text{hnf}} {v_1}^2}{k ¥_\infty}. \tag{6.1}$$

Entropy analysis has the following non-dimensional formula [91]:

$$N_G = \frac{¥_\infty^2 b^2 E_G}{k_f(¥_w - ¥_\infty)^2}. \quad (6.2)$$

By formula (3.2), the non-dimensional entropy formula is:

$$N_G = R_e\left[\phi_d(1 + N_r)\theta'^2 + \frac{1}{\phi_a}\frac{B_r}{\Omega}(f''^2 + Kf'^2)\right], \quad (6.3)$$

where R_e represents the Reynolds number, Brinkmann number is represented by B_r, and Ω symbolizes the dimensionless temperature gradient.

7 Results and discussion

The discussion is based on the numerical outcomes attained from the considered model that are itemized in the previous part. The implied parameters in this section are λ, A, K, ϕ, Λ, N_r, B_i, E_c, Q, S, R_e, and B_r. Physical performance of dimensionless parameters including entropy, swiftness, and temperature is shown in Figures 3–22. Outcomes for Cu–EO conventional SBNF and GO–Cu/EO non-Newtonian SBHNF are attained. Coefficients of drag force along with temperature variations are described in Table 5. Following are default values $\lambda = 0.1$, $A = 0.2$, $K = 0.1$, $\phi = 0.18$, $\phi_H = 0.09$, $\Lambda = 0.3$, $n = 0.2$, $Q = 0.3$, $P_r = 7.38$, $N_r = 0.3$, $B_i = 0.2$, $E_c = 0.2$, $R_e = 5$, $B_r = 5$, and $S = 0.1$. The effects of Deborah number λ on temperature, entropy outlines, and swiftness of Cu–EO mono SBNF and GO–Cu/EO SBHNF are displayed in Figures 3–5. Calculations are accomplished for $\lambda = 0.1$, 0.2, 0.3 at orderly nanoparticles concentration of $\phi_R = 0.09$, $\phi_H = 0.09$, and $\phi = 0.18$. The swiftness is enhanced when values of λ are raised as shown in Figure 3. So the thickness of the impetus boundary layer is increased. Increment in λ resulted in reducing the velocity profile which caused the momentum of the border sheet to reduce. Motion of the fluid decreases due to resistance. At $\lambda = 0.1$, GO–Cu/EO hybrid nanoliquid has a comparatively higher thickness of boundary-layer than the Cu–EO nanoliquid. The growing

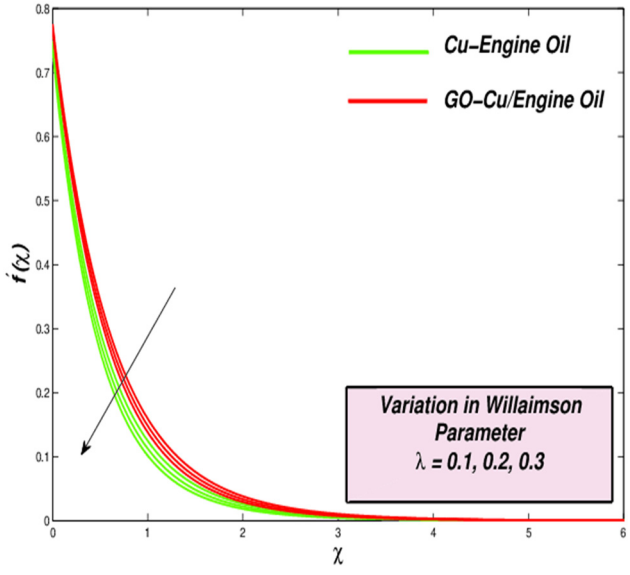

Figure 3: Velocity variation *vs* λ.

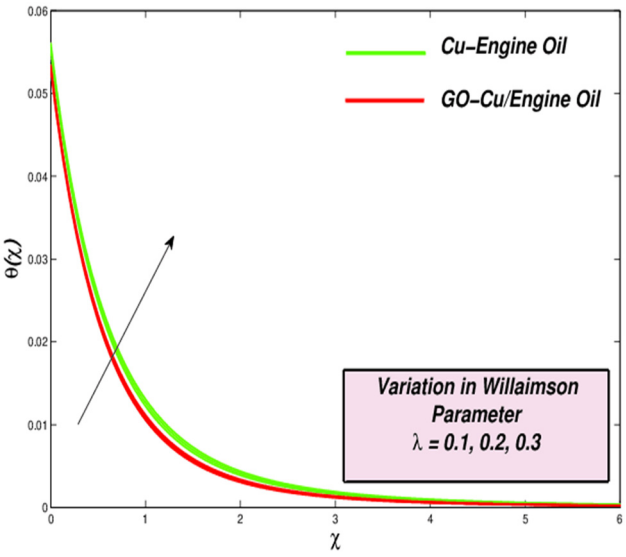

Figure 4: Temperature variation *vs* λ.

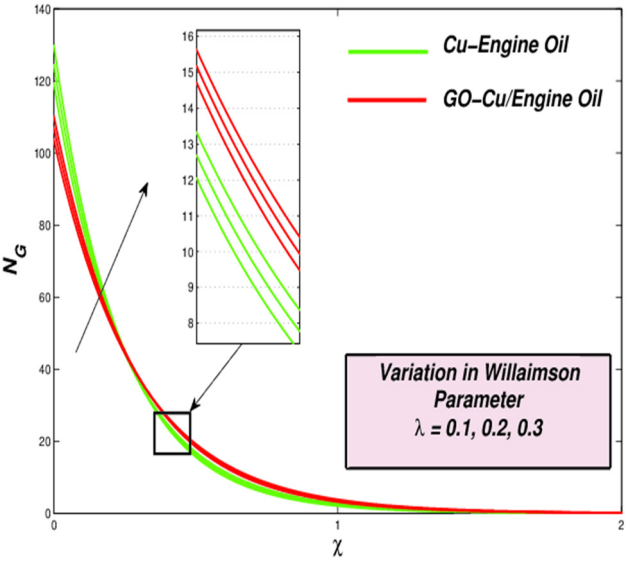

Figure 5: Entropy variation *vs* λ.

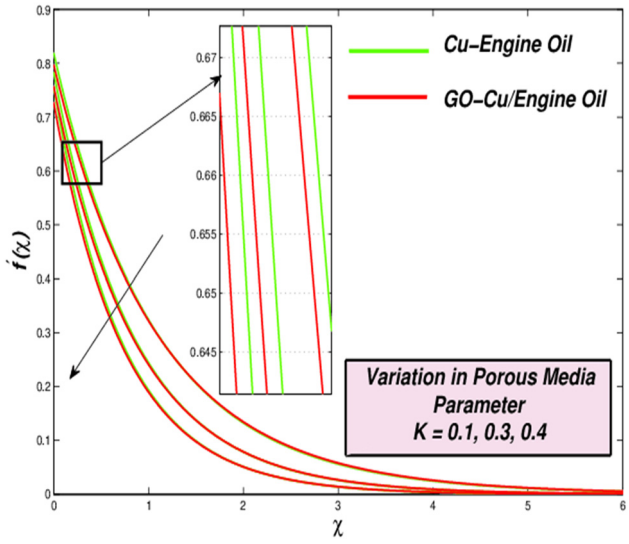

Figure 6: Velocity change with K.

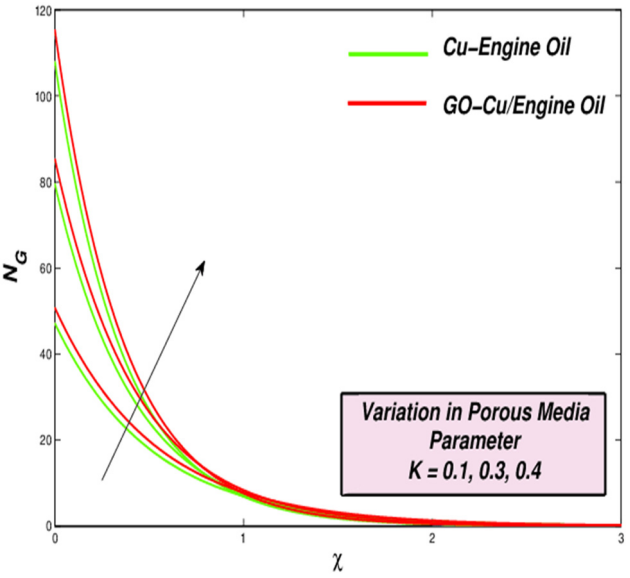

Figure 8: Entropy variations against K.

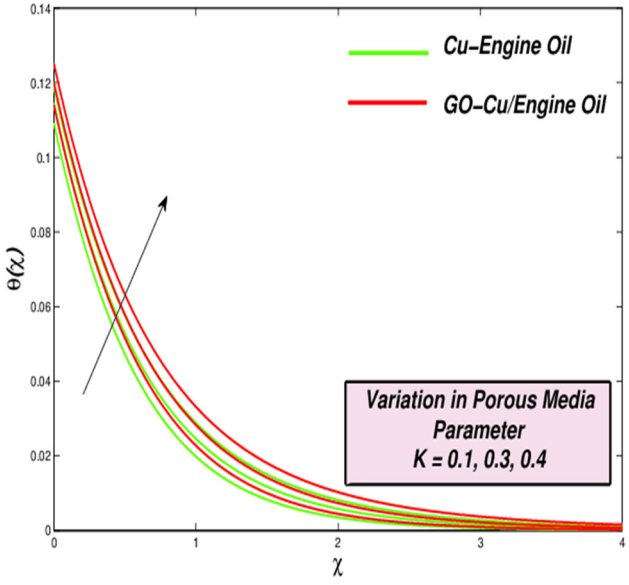

Figure 7: Temperature change with K.

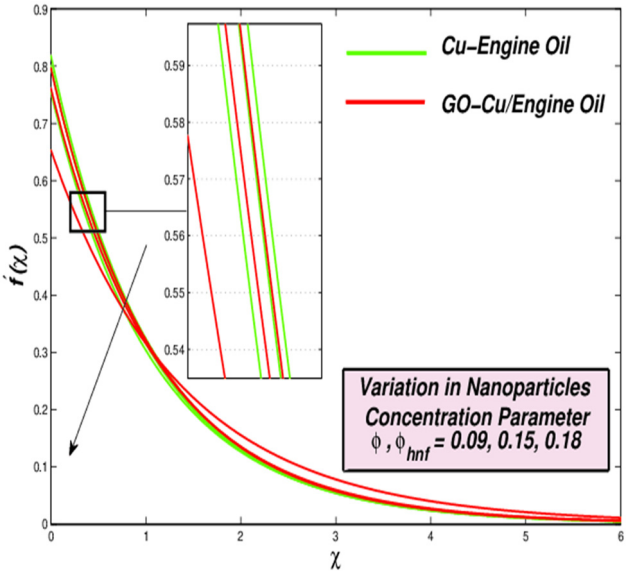

Figure 9: Velocity variation *vs* ϕ and ϕ_{hnf}.

value of the resilience-stress variable resulted in increasing the heat in the boundary layer as shown in Figure 4. The rate of heat transfer, as depicted by Nusselt number, decreases for Cu–EO as well as for GO–Cu/EO. Increment in system entropy is observed with increase in the values of λ, as displayed in Figure 5. The behavioral shifts in the velocity and temperature of hybrid nanoliquid are seen in Figures 6 and 7. The amplitude of the resistive body force decreases with the increase in permeability, so a constant reduction in drag is confronted with fluid, and the flow decreases so that the speed in that borderline tends to zero. The vector K affects the nanofluid density directly by reducing the fluid temperature inside the border layer, leading to a reduction in the fluid permeability of the medium. Entropy of system likewise upsurges, in this case, Figure 8. Increment in variable K increases the heat transfer rate. The influence of nanoparticles size ϕ of mono-nanofluids and ϕ_{hnf} of hybrid-nanofluids are depicted in Figures 9 and 10. Here $\phi_{\text{R}} = 0.09$, so analysis is done for varied values of ϕ_{H}. Increment in the values of ϕ and ϕ_{hnf} resulted in the velocity profile of nanofluids decreasing.

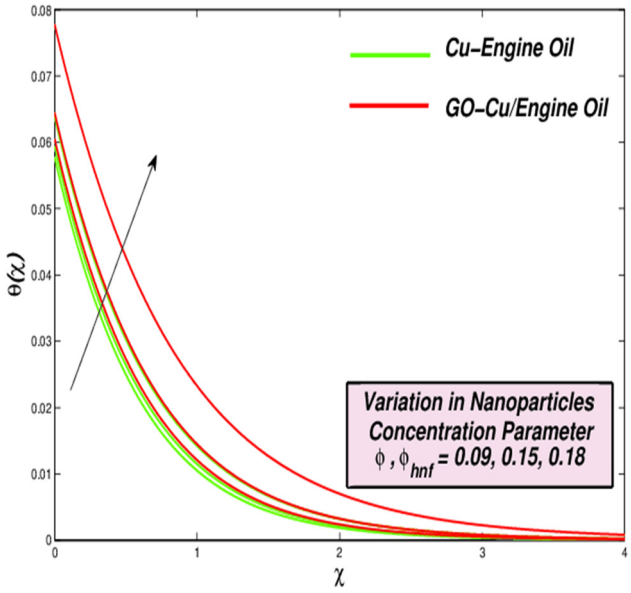

Figure 10: Temperature variations with ϕ and ϕ_{hnf}.

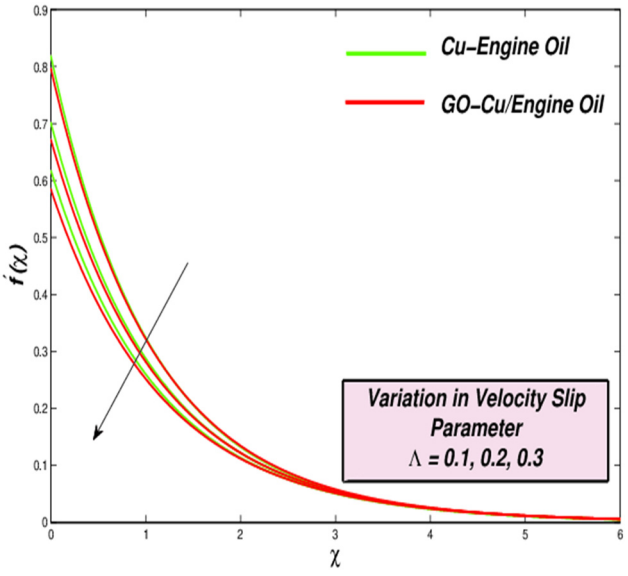

Figure 12: Velocity variations with Λ.

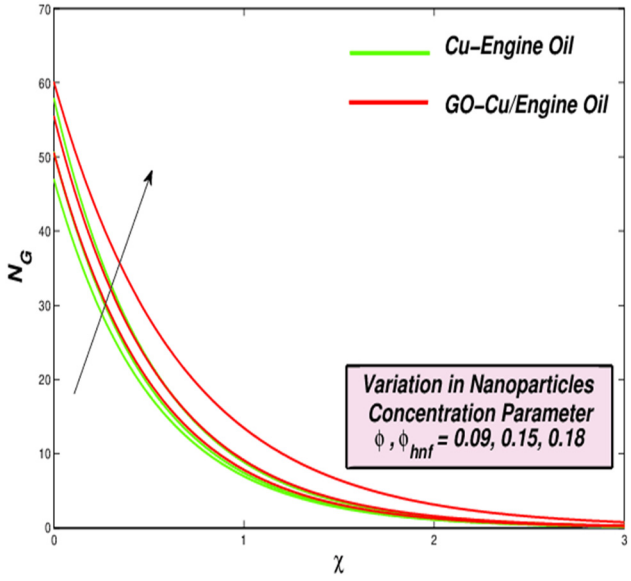

Figure 11: Entropy variations with ϕ and ϕ_{hnf}.

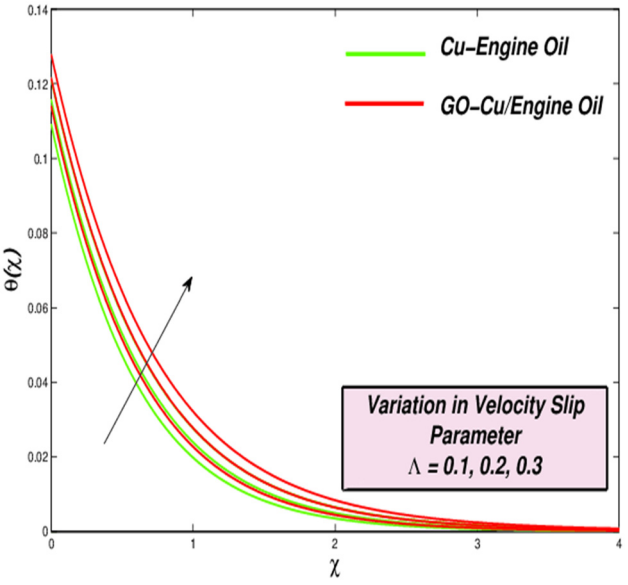

Figure 13: Temperature variations with Λ.

Meanwhile, a profile of temperature is observed to be elevated. The variable ϕ and ϕ_{hnf} are representing solid nanoparticles volume inside basefluid. As there is a higher thermal conductance in solid-molecules than in traditional liquids, increment in the values of ϕ and ϕ_{hnf} resulted in decreasing the velocity profile of the fluid as shown in Figure 9. Temperature profile in the boundary layer also increases. Figure 12 displays the thickness of the thermal boundary layer to increase with increment in the net thermal conductance of nanofluids. Temperature profile of hybrid nanofluids rises at a higher rate as compared with conventional nanofluids. Figure 11 illustrates that entropy is improved for larger solid nanomolecule sizes. For SBNF and SBHNF, Figures 12–14 show the effect of slippery parameter on the flowing, temperature, and entropy producing outlines, respectively. For the slippery behavior Λ, decreasing behavior in velocity is evident, as the slippery effect decelerated the fluid flowing. The thermal energy of the fluid has an opposite effect as nanofluid temperatures rise with an increase in the variable

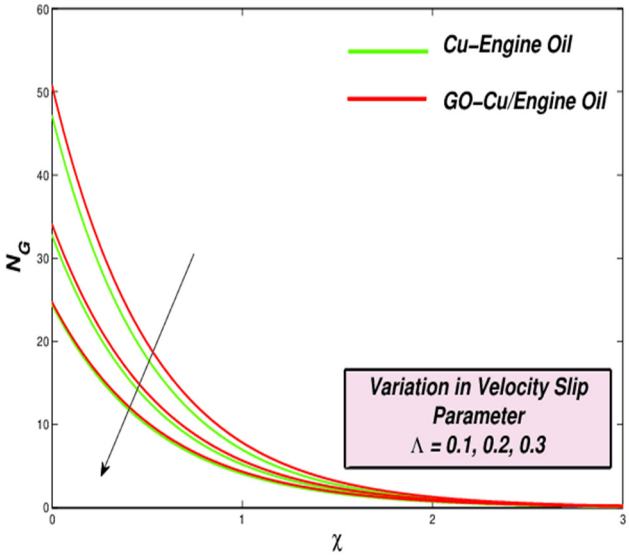

Figure 14: Entropy variations with Λ.

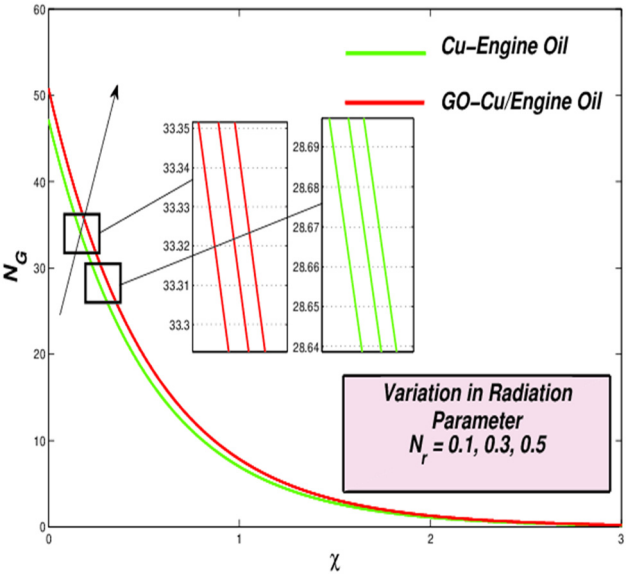

Figure 16: Entropy variations *vs* N_r.

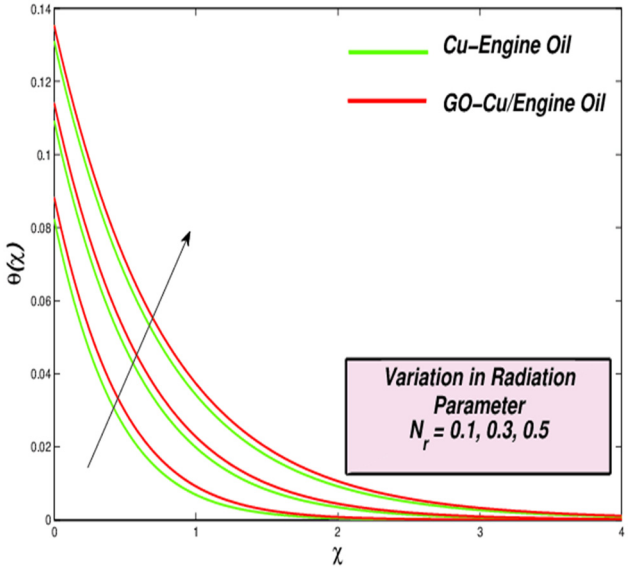

Figure 15: Temperature variations *vs* N_r.

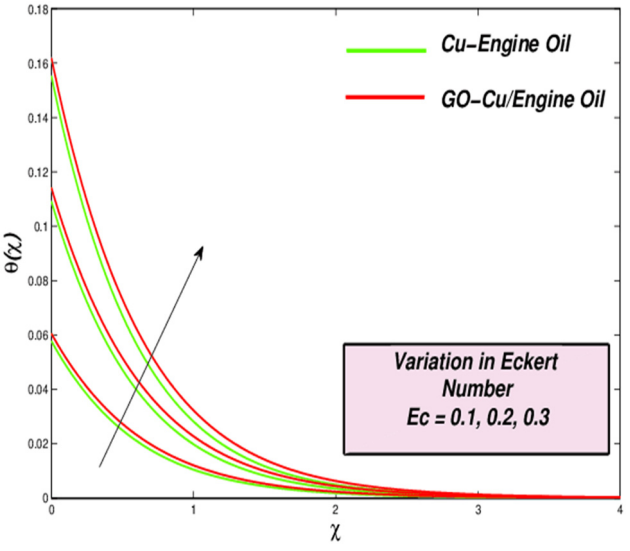

Figure 17: Temperature variations *vs* E_c.

energy Figure 13. Owing to the increased slip parameter Λ, there is a reduction in the drag force between the fluid and its borders. From Figure 14, the entropy is decreased with rising values of Λ, it can be quickly remarked. Larger Λ values mean that the boundary-layer has a reduced velocity. This decreases the velocity in exchange for reducing the frictional forces within fluid friction, which also reduces frictional irreversibility. Thus, its relation to entropy is reduced by entropy, which reduces the entropy of the system. Figure 15 illustrates how the thermal radiation variable impacts the thermal outlines of SBNF and SBHNF, which shows that the nanofluid temperatures are increased for increasing amounts of N_r = 0.1, 0.3, 0.5. The increased heating rate behavior as shown in Table 5 would also contribute to an improvement in thermal rendering and efficacy. If the temperature is boosted, the thickness of the thermal boundary-layer is enhanced. This is because there is a higher heat fluxing. Moreover, heat dissipative transfer E_c is the kinetic energy to the gap ratio to the boundary-layer enthalpy. Higher value of E_c indicates greater kinetic energy, meanwhile, the friction causes heating on the sheet,

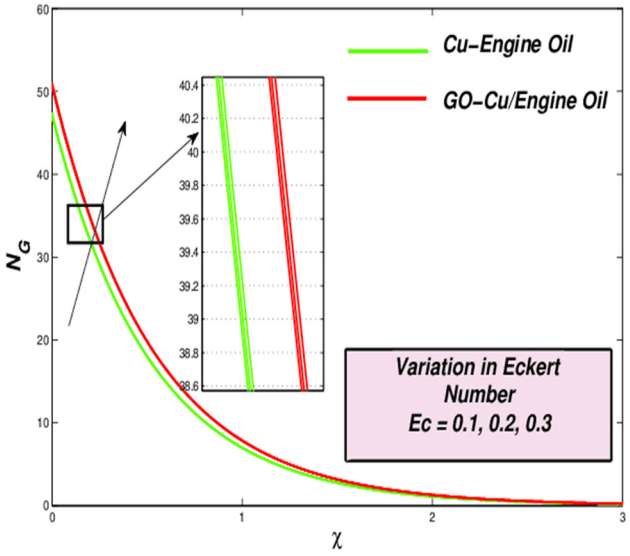

Figure 18: Entropy variations *vs* E_c.

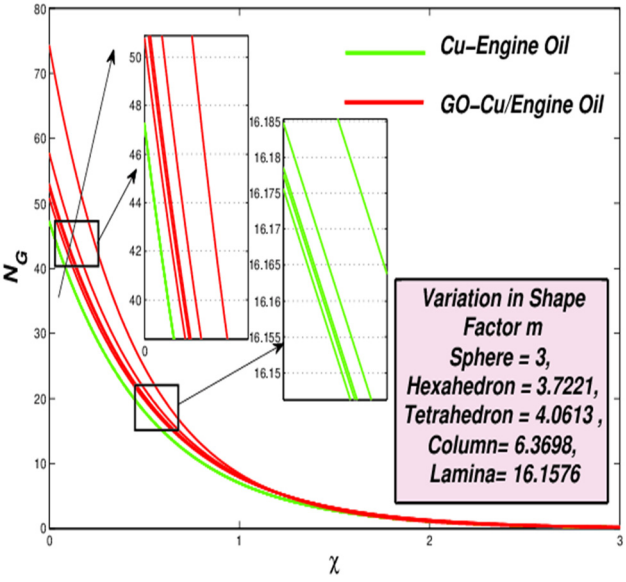

Figure 20: Entropy variations with variable *m*.

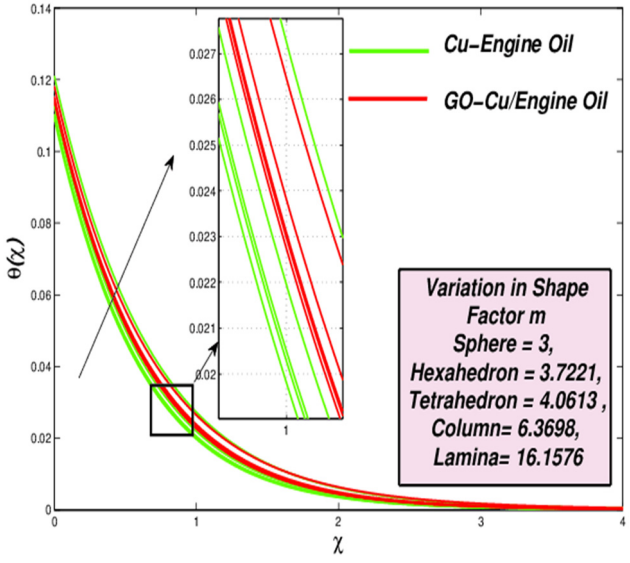

Figure 19: Temperature variations with *m*.

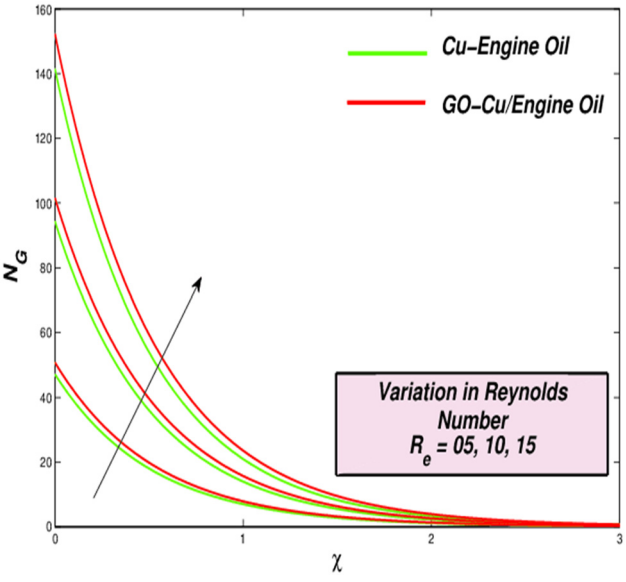

Figure 21: Entropy variations *vs* R_e.

which resulted in raising the temperature of the liquid. Figure 17 shows the improvement in temperature with increasing values of E_c. The increment in N_r and E_c parameters can be seen in Figures 16 and 18, respectively on the entropy distribution. According to Table 5, the rate of heat transfer increases for N_r and E_c in both nanofluids (GO–Cu/EO and Cu–EO), while the gradient of the velocity profile is constant at the plate. Thermal efficiency of the system has a vital role in the shape of nanoparticles. According to the researchers, the surface area of nanoparticles has a major role in increasing or decreasing the heat transfer rate. Analysis is done on the effect of solid nanoparticles on the temperature and system entropy. Figures 19 and 20 show the findings for five different shapes of the nanoparticle. Figure 19 shows the values of the shape-factor while using a different shape. The temperature is boosted for an increased amount of m as seen in Figure 20. In addition, for $m = 3$, *i.e.*, spherical nanoparticles, the lowest interface temperature is noticed. It is the result of the net surface area of the sphere along with the highest heat transfer rate of fluid into the inner fluid from the surface. This is

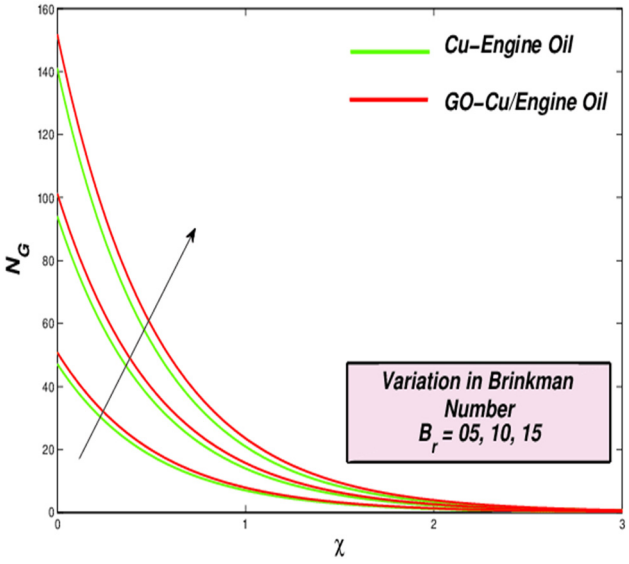

Figure 22: Entropy variations *vs* B_r.

also verified by the surface heat transmission coefficient in Table 5. In Figure 22, entropy is boosted with increasing values of m. In the spherical-shaped particles, it is obvious that entropy has the smallest rate. Lastly, Reynolds R_e and Brinkmann B_r numbers' impacts are provided on entropy production. The R_e value raises the entropy to depend on the outcomes. The interpretation: the inertial forces overpower viscid effects when the R_e values are high. As seen in Figure 21, the thermal scheme production of entropy thus boosts. The effect of B_r on entropy is shown in Figure 22, where the increase in B_r increased the entropy production. The fact is that the rise in B_r means more heat is dissipated than heat is carried on the surface and entropy is augmented.

8 Final results and future guidance

In the current analysis, a permeable stretched surface was carried out to calculate the boundary-layer flow of non-Newtonian EO based on Cu and GO hybrid nanofluids. The KBM was employed in an investigation in the presence of porous regime, viscidness dissipative flowing, form, entropy, and thermal radiative impact. The above procedure has the following summary:

Table 5: Values of $C_f Re_x^{1/2}$ and $Nu_x Re_x^{-1/2}$ for $P_r = 6, 450$ and $n = 0.2$

λ	S	K	ϕ	ϕ_H	Λ	E_c	N_r	B_i	$C_f Re_x^{\frac{1}{2}}$ Cu–EO	$C_f Re_x^{\frac{1}{2}}$ GO–Cu/EO	$N_u Re_x^{\frac{-1}{2}}$ Cu–EO	$N_u Re_x^{\frac{-1}{2}}$ GO–Cu/EO
0.1	0.1	0.1	0.18	0.09	0.3	0.2	0.3	0.2	1.1833	1.2678	0.1412	0.1623
0.2									0.1602	1.2589	0.1203	0.1564
0.3									0.1487	1.2321	0.1134	0.1461
	0.1								1.1833	1.2678	0.1412	0.1623
	0.2								1.1920	1.2701	0.1648	0.1789
	0.3								1.2161	1.3054	0.1787	0.1831
		0.1							1.1833	1.2678	0.1412	0.1623
		0.3							1.5055	1.6088	0.1283	0.1290
		0.4							1.7526	1.8692	0.1267	0.1273
			0.09						0.1721	—	0.0978	—
			0.15						0.1765	—	0.1129	—
			0.18						1.1833	—	0.1412	—
				0.0					—	0.1721	—	0.0978
				0.06					—	1.1860	—	0.1344
				0.09					—	1.2678	—	0.1623
					0.1				2.0156	2.2401	0.1609	0.1984
					0.2				1.2316	2.1945	0.1588	0.1793
					0.3				1.1833	1.2678	0.1412	0.1623
						0.1			1.1833	1.2678	0.1335	0.1407
						0.2			1.1833	1.2678	0.1412	0.1623
						0.3			1.1833	1.2678	0.1612	0.1820
							0.1		1.1833	1.2678	0.1298	0.1450
							0.3		1.1833	1.2678	0.1412	0.1623
							0.5		1.1833	1.2678	0.1553	0.1756
								0.1	1.1833	1.2678	0.1288	0.1356
								0.2	1.1833	1.2678	0.1412	0.1623
								0.3	1.1833	1.2678	0.1618	0.1829

1) The temperature profile is raised with λ, K, ϕ, ϕ_{hnf}, E_{c}, B_i, and N_{r} parameters, while it is declined with Λ.
2) Velocity is diminished with a swelling impact of λ, ϕ, and ϕ_{hnf}.
3) Entropy is raised with augmentation in λ, A, K, ϕ, E_{c} B_i, N_{r}, $S > 0$, B_{r}, and R_{e}, while it is diminished with the increment in Λ, hence the thermal efficiency of the model is enhanced.
4) For sphere-shaped nanosolid-particles, the utmost heat transport is seen, while for lamina-shaped nanosolid-particles, a lower heat transport is noticed.
5) According to the current study, Cu-GO/EO hybrid nanofluid is more eminent than Cu/EO in heat transmission.

The results of this analysis can be used as guidance for future research, in which thermal efficacy can be calculated by using various kinds of mixture of non-Newtonian nanoliquids (*i.e,*. Casson, Falkner–Skan, micropolar, Eyring–Powell, *etc*.). Furthermore, equations may be generalized to include the effects of the viscidity based on temperature, porousness depending on temperatures, and magneto multi-dimensional slippery flowing.

Acknowledgment: Taif University Researchers Supporting Project number (TURSP-2020/319), Taif University, Taif, Saudi Arabia.

Funding information: Taif University.

Author contributions: All authors have accepted responsibility for the entire content of this manuscript and approved its submission.

Conflict of interest: The authors state no conflict of interest.

References

[1] Buongiorno J. Convective transport in nanofluids. ASME J Heat Transf. 2006;128:240–50.
[2] Khoa YB, Hussananb A, Mohameda MKA, Salleha MZ. Heat and mass transfer analysis on flow of Williamson nanofluid with thermal and velocity slips: Buongiorno model. Propuls Power Res. 2019;8(3):243–52.
[3] Garoosi F, Garoosi S, Hooman K. Numerical simulation of natural convection and mixed convection of the nanofluid in a square cavity using Buongiorno model. Powder Technol. 2014;268(9):279–92.
[4] Eiamsa-ard S, Kiatkittipong K, Jedsadaratanachai W. Heat transfer enhancement of TiO_2/water nanofluid in a heat exchanger tube equipped with overlapped dual twisted-tapes. Eng Sci Technol. 2015;18:336–50.
[5] Eid MR. Effects of NP shapes on non-Newtonian bio-nanofluid flow in suction/blowing process with convective condition: Sisko model. J Non-Equili Thermodyn. 2020;45(2):97–108.
[6] Eid MR. Thermal characteristics of 3D nanofluid flow over a convectively heated Riga surface in a Darcy–Forchheimer porous material with linear thermal radiation: an optimal analysis. Arab J Sci Eng. 2020;45(11):9803–14.
[7] Tarakaramu N, Narayana PVS, Venkateswarlu B. Numerical simulation of variable thermal conductivity on 3D flow of nanofluid over a stretching sheet. Nonlinear Eng. 2020;9(1):233–43.
[8] Heshmati F, Ertuk H. Single-phase models for improved estimation of friction factor for laminar nanofluid flow in pipes. Int J Heat Mass Transf. 2016;95:416–25.
[9] Maiga SEB, Nguyen CT, Galanis N, Roy G. Heat transfer behaviours of nanofluids in a uniformly heated tube. Superlattices Microstruct. 2004;35:543–57.
[10] Palm SJ, Roy G, Nguyen CT. Heat transfer enhancement with the use of nanofluids in radial flow cooling systems considering temperature dependent features. Appl Therm Eng. 2006;26(17–18):2209–18.
[11] Xuan Y, Roetzel W. Conceptions for heat transfer correlation of nanofluids. Int J Heat Mass Transf. 2000;43(19):3701–7.
[12] Heris SZ, Esfahany MN, Etemad G. Numerical investigation of nanofluid laminar convective heat transfer through a circular tube. Numer Heat Transf Part A. 2007;52(11):1043–58.
[13] Mokmeli A, Avval MS. Prediction of nanofluid convective heat transfer using the dispersion model. Int J Therm Sci. 2010;49(3):471–8.
[14] Alaidrous AA, Eid MR. 3-D electromagnetic radiative non-Newtonian nanofluid flow with Joule heating and higher-order reactions in porous materials. Sci Rep. 2020;10(1):14513.
[15] Mabood F, Yusuf TA, Bognar G. Features of entropy optimization on MHD couple stress nanofluid slip flow with melting heat transfer and nonlinear thermal radiation. Sci Rep. 2020;10:19163.
[16] Gul N, Ramzan M, Chung JD, Kadry S, Chu YM. Impact of hall and ion slip in a thermally stratified nanofluid flow comprising Cu and Al_2O_3 nanoparticles with nonuniform source/sink. Sci Rep. 2020;10:18064.
[17] Pushpa BV, Sankar M, Mebarek-Oudina F. Buoyant convective flow and heat dissipation of Cu–H_2O nanoliquids in an annulus through a thin baffle. J Nanofluids. 2020;10(2):292–304.
[18] Dadheech PK, Agrawal P, Mebarek-Oudina F, Abu-Hamdeh NH, Sharma A. Comparative heat transfer analysis of $MoS_2/C_2H_6O_2$ and SiO_2-$MoS_2/C_2H_6O_2$ nanofluids with natural convection and inclined magnetic Field. J Nanofluids. 2020;9(3):161–7.
[19] Swain K, Mahanthesh B, Mebarek-Oudina F. Heat transport and stagnation-point flow of magnetized nanoliquid with variable thermal conductivity, Brownian moment and thermophoresis aspects. Heat Transf - Asian Res. 2021;50(1):754–67.
[20] Warke AS, Ramesh K, Mebarek-Oudina F, Abidi A. Numerical investigation of the stagnation point flow of radiative magnetomicropolar liquid past a heated porous stretching sheet. J Therm Anal Calorim. 2021.
[21] Dhif K, Mebarek-Oudina F, Chouf S, Vaidya H, Chamkha AJ. Thermal analysis of the solar collector cum storage system using a hybrid-nanofluid. J Nanofluids. 2021;10(4):616–26.

[22] Mahanthesh B, Lorenzini G, Oudina FM, Animasaun IL. Significance of exponential space-and thermal-dependent heat source effects on nanofluid flow due to radially elongated disk with Coriolis and Lorentz forces. J Therm Anal Calorim. 2020;141(1):37–44.
[23] Asogwa KK, Mebarek-Oudina F, Animasaun I. Comparative investigation of water-based Al_2O_3 nanoparticles through water-based CuO nanoparticles over an exponentially accelerated radiative Riga plate surface *via* heat transport. Arab J Sci Eng. 2022;1–18.
[24] Radouane F, Aissa A, Mebarek-Oudina F, Ahmed W, Rashad AM, Sahnoun M, et al. Magneto-free convective of hybrid nanofluid inside non-darcy porous enclosure containing an adiabatic rotating cylinder. Energy Sources A: Recovery Util Environ Eff. 2020.
[25] Redouane F, Jamshed W, Devi SU, Prakash M, Nisar KS, Nasir NAAMOHD, et al. Galerkin finite element study for mixed convection (TiO_2-SiO_2/Water) hybrid-nanofluidic flow in a triangular aperture heated beneath. Sci Rep. 2021;11:22905.
[26] Amine BM, Redouane F, Mourad L, Jamshed W, Eid MR, Al-Kouz W. Magnetohydrodynamics natural convection of a triangular cavity involving Ag-MgO/Water hybrid nanofluid and provided with rotating circular barrier and a quarter circular porous medium at its right-angled corner. Arab J Sci Eng. 2021;46:12573–97.
[27] Hiba B, Redouane F, Jamshed W, Saleel CA, Devi SU, Prakash M, et al. A novel case study of thermal and streamline analysis in a grooved enclosure filled with (Ag–MgO/Water) hybrid nanofluid: Galerkin FEM. Case Stud Therm Eng. 2021;27:101372.
[28] Animasaun I, Yook S-J, Muhammad T, Mathew A. Dynamics of ternary-hybrid nanofluid subject to magnetic flux density and heat source or sink on a convectively heated surface. Surfaces Interfaces. 2022;28:101654.
[29] Jamshed W, Eid MR, Mohd Nasir NAA, Nisar KS, Aziz A, Shahzad F, et al. Thermal examination of renewable solar energy in parabolic trough solar collector utilizing Maxwell nanofluid: a noble case study. Case Stud Therm Eng. 2021;27:101258.
[30] Akram J, Akbar NS, Tripathi D. Blood-based graphene oxide nanofluid flow through capillary in the presence of electromagnetic fields: a Sutterby fluid model. Microvascular Res. 2020;132:104062.
[31] Hayat T, Ahmad S, Khan MI, Alsaedi A. Modeling chemically reactive flow of Sutterby nanofluid by a rotating disk in presence of heat generation/absorption. Commun Theoret Phys. 2018;69:569.
[32] Khan WA, Ali M, Waqas M, Shahzad M, Sultan F, Irfan M. Importance of convective heat transfer in flow of non-Newtonian nanofluid featuring Brownian and thermophoretic diffusions. Int J Numer Meth Heat Fluid Flow. 2019;29:4624–41.
[33] Hashim A, Hamid MK. Unsteady mixed convective flow of Williamson nanofluid with heat transfer in the presence of variable thermal conductivity and magnetic field. J Mol Liq. 2018;260:436–46.
[34] Aziz A, Jamshed W. Unsteady MHD slip flow of non-Newtonian Power-law nanofluid over a moving surface with temperature dependent thermal conductivity. Discrete Contin Dyn Syst Ser A. 2018;11:617–30.
[35] Asif M, Jamshed W, Asim A. Entropy and heat transfer analysis using Cattaneo–Christov heat flux model for a boundary layer flow of Casson nanofluid. Result Phys. 2018;4:640–9.
[36] Mukhtar T, Jamshed W, Aziz A, Kouz WA. Computational investigation of heat transfer in a flow subjected to magnetohydrodynamic of Maxwell nanofluid over a stretched flat sheet with thermal radiation. Numer Meth Part Differ Eq. 2020. doi: 10.1002/num.22643.
[37] Jamshed W, Shahzad F, Safdar R, Sajid T, Eid MR, Nisar KS. Implementing renewable solar energy in presence of Maxwell nanofluid in parabolic trough solar collector: a computational study. Waves Random Complex Media. 2021.
[38] Al-Dhaifallah M, Nassef AM, Rezk H, Nisar KS. Optimal parameter design of fractional order control based INC-MPPT for PV system. Sol Energy. 2018;159:650–64.
[39] Mohyud-Din Adnan TS, Khan U, Ahmed N, Khan I, Abdeljawad T, Nisar KS. Thermal transport investigation in magneto-radiative GO-MoS_2/H_2O-$C_2H_6O_2$ hybrid nanofluid subject to Cattaneo–Christov model. Molecules. 2020;25(11):2592.
[40] Jamshed W, Nisar KS. Computational single phase comparative study of Williamson nanofluid in parabolic trough solar collector *via* Keller-box method. Int J Energy Res. 2021;45(7):10696–718.
[41] Jamshed W, Baleaznu D, Mohd Nasir NAA, Shahzad F, Nisar KS, Shoaib M, et al. The improved thermal efficiency of Prandtl–Eyring hybrid nanofluid *via* classical Keller-box technique. Sci Rep. 2021;11:23535.
[42] Lund LA, Ching DLC, Omar Z, Khan I, Nisar KS. Triple local similarity solutions of Darcy-Forchheimer magnetohydrodynamic (MHD) flow of micropolar nanofluid over an exponential shrinking surface: stability analysis. Coatings. 2019;9(8):527.
[43] Rasool G, Shafiq A, Khan I, Baleanu D, Nisar KS, Shahzadi G. Entropy generation and consequences of MHD in Darcy–Forchheimer nanofluid flow bounded by non-linearly stretching surface. Symmetry. 2020;12(4):652.
[44] Tassaddiq A, Khan I, Nisar KS. Heat transfer analysis in sodium alginate based nanofluid using MoS2 nanoparticles: Atangana–Baleanu fractional model. Chaos, Solitons & Fractals. 2020;130:109445.
[45] Jayadevamurthy PGR, Rangaswamy NK, Prasannakumara BC, Nisar KS. Emphasis on unsteady dynamics of bioconvective hybrid nanofluid flow over an upward–downward moving rotating disk. Numer Methods Partial Differ Equ. 2020.
[46] Sheikh NA, Ching DLC, Khan I, Kumar D, Nisar KS. A new model of fractional Casson fluid based on generalized Fick's and Fourier's laws together with heat and mass transfer. Alex Eng J. 2020;59(5):2865–76.
[47] Shahzad F, Jamshed W, Sajid T, Nisar KS, Eid MR. Heat transfer analysis of MHD rotating flow of Fe_3O_4 nanoparticles through a stretchable surface. Commun Theor Phys. 2021;73:075004.
[48] Jamshed W, Devi SU, Goodarzi M, Prakash M, Nisar KS, Zakarya M, et al. Evaluating the unsteady Casson nanofluid over a stretching sheet with solar thermal radiation: An optimal case study. Therm Eng. 2021;26:101160.
[49] Suresh S, Venkitaraj K, Selvakumar P, Chandrasekar M. Experimental investigation of mixed convection with synthesis of Al_2O_3-water hybrid nanofluids using two step method and its thermo physical properties. Collo Surf. 2011;8:41–8.
[50] Devi SSU, Devi SPA. Numerical investigation on three dimensional hybrid Cu–Al_2O_3/water nanofluid flow over a stretching

sheet with effecting Lorentz force subject to Newtonian heatings. Can J Phys. 2016;94:490–6.
[51] Afrand M, Toghraie D, Ruhani B. Effects of temperature and nanoparticles concentration on rheological behavior of Fe_3O_4-Ag/EG hybrid nanofluid: an experimental study. Exp Therm Fluid Sci. 2016;77:38–44.
[52] Hayat T, Nadeem S. Heat transfer enhancement with Ag–CuO/water hybrid nanofluid. Results Phys. 2017;7:2317–24.
[53] Ghadikolaei SS, Yassari M, Hosseinzadeh K, Ganji DD. Investigation on thermophysical properties of TiO_2–Cu/H_2O hybrid nanofluid transport dependent on shape factor in MHD stagnation point flow. Powder Technol. 2017;322:428–4358.
[54] Hussain S, Ahmed SE, Akbar T. Investigation on thermophysical properties of TiO_2–Cu/H_2O hybrid nanofluid transport dependent on shape factor in MHD stagnation point flow. Int J Heat Mass Transf. 2017;114:1054–66.
[55] Al-Hossainy AF, Eid MR. Combined experimental thin films, TDDFT-DFT theoretical method, and spin effect on $[PEG\text{-}H_2O/ZrO_2 + MgO]^h$ hybrid nanofluid flow with higher chemical rate. Surf Interfaces. 2021;23:100971.
[56] Eid MR, Al-Hossainy AF. Combined experimental thin film, DFT-TDDFT computational study, flow and heat transfer in $[PG\text{-}MoS_2/ZrO_2]^C$ hybrid nanofluid. Waves Complex Media. 2021;1–26. doi: 10.1080/17455030.2021.1873455.
[57] Jamshed W, Aziz A. Cattaneo–Christov based study of TiO_2–CuO/H_2O Casson hybrid nanofluid flow over a stretching surface with entropy generation. Appl Nanosci. 2018;8:685–98.
[58] Aziz A, Jamshed W, Ali Y, Shams M. Heat transfer and entropy analysis of Maxwell Hybrid nanfluid including effects of inclined magnetic field, joule heating and thermal radiation. J Discrete Contin Dyn Sys. 2020;13(10):2667–90.
[59] Aziz A, Jamshed W, Aziz T, Bahaidarah HMS, Ur Rehman K. Entropy analysis of Powell-Eyring hybrid nanofluid including effect of linear thermal radiation and viscous dissipation. J Therm Anal Calorim. 2020;143:1331.
[60] Mahian O, Mahmud S, Pop I. Analysis of first and second laws of thermodynamics between two isothermal cylinders with relative rotation in the presence of MHD flow. Int J Heat Mass Transf. 2012;55(17–18):4808–16.
[61] Mahian O, Kianifar A, Kleinstreuer C, Al-Nimr MA, Pop I, Sahin AZ, et al. A review of entropy generation in nanofluid flow. Int J Heat Mass Transf. 2013;65:514–32.
[62] Cengel YA, Boles MA. Thermodynamics an Engineering Approach. Fifth ed. New York City, U.S.: McGraw-Hill; 2006.
[63] Oztop HF, Salem KA. A review on entropy generation in natural and mixed convection heat transfer for energy systems. Renew Sustain Energy Rev. 2012;16(1):911–20.
[64] Shahzad A, Ali R, Hussian M, Kamran MS. Unsteady axisymmetric flow and heat transfer over time dependent radially stretching sheet. Alex Eng J. 2017;56:35–41.
[65] Mehrali M, Sadeghinezhad E, Akhiani AR, Latibari ST, Metselaar HSC, Kherbeet AS, et al. Heat transfer and entropy generation analysis of hybrid graphene/Fe_3O_4 ferro-nanofluid flow under the influence of a magnetic field. Powder Tech. 2017;308:149–57.
[66] Shahzad A, Ali R, Hussian M, Kamran MS. Entropy generation in a second grade magnetohydrodynamic nanofluid flow over a convectively heated stretching sheet with nonlinear thermal radiation and viscous dissipation. Results Phys. 2018;9:1077–85.
[67] Huminic G, Huminic A. The heat transfer performances and entropy generation analysis of hybrid nanofluids in a flattened tube. Int J Heat Mass Transf. 2018;119:813–27.
[68] Eid MR, Mabood F. Entropy analysis of a hydromagnetic micropolar dusty carbon NTs-kerosene nanofluid with heat generation: Darcy–Forchheimer scheme. J Therm Anal Calorim. 2020;143:2419–36.
[69] Li Z, Sheikholeslami M, Jafaryar M, Chamkha AJ. Investigation of nanofluid entropy generation in a heat exchanger with helical twisted tapes. J Mol Liq. 2018;266:797–805.
[70] Hanif H, Khan I, Shafie S. Heat transfer exaggeration and entropy analysis in magneto-hybrid nanofluid flow over a vertical cone: a numerical study. J Therm Anal Calorim 141(2020):2001–17.
[71] Eid MR, Mabood F. Two-phase permeable non-Newtonian cross-nanomaterial flow with arrhenius energy and entropy generation: Darcy-Forchheimer model. Phys Scr. 2020;95(10):105209.
[72] Khan ZH, Khan WA, Hamid M, Liu H. Finite element analysis of hybrid nanofluid flow and heat transfer in a split lid-driven square cavity with Y-shaped obstacle. Phys Fluids. 2020;32(9):093609.
[73] Mourad A, Aissa A, Mebarek-Oudina F, Jamshed W, Ahmed W, Ali HM, et al. Galerkin finite element analysis of thermal aspects of Fe_3O_4-MWCNT/water hybrid nanofluid filled in wavy enclosure with uniform magnetic field effect. Int Commun Heat Mass Transf. 2021;126:105461.
[74] Rana P, Makkar V, Gupta G. Finite element study of bio-convective Stefan blowing Ag-MgO/water hybrid nanofluid induced by stretching cylinder utilizing non-Fourier and non-Fick's laws. Nanomaterials. 2021;11(7):1735.
[75] Shah Z, Saeed A, Khan I, Selim MM, Kumam P. Numerical modeling on hybrid nanofluid (Fe3O4 + MWCNT/H2O) migration considering MHD effect over a porous cylinder. PLoS One. 2021;16(7):e0251744.
[76] Nasrin R, Hossain S, Zahan I, Ahmed KFU, Fayaz H. Performance analysis of hybrid/single nanofluids on augmentation of heat transport in lid-driven undulated cavity. Heat Transf. 2020;49(8):4204–25.
[77] Tiwari RJ, Das MK. Heat transfer augmentation in a two-sided lid-driven differentially heated square cavity utilizing nanofluids. Int J Heat Mass Transf. 2007;50(9–10):2002–18.
[78] Hayat T, Qasim M, Mesloub S. MHD flow and heat transfer over permeable stretching sheet with slip conditions. Int J Numer Meth Fluids. 2011;566:963–75.
[79] Bilal S, Sohail M, Naz R, Malik MY, Alghamdi M. Upshot of Ohmically dissipated Darcy-Forchheimer slip flow of magnetohydrodynamic Sutterby fluid over radiating linearly stretched surface in view of Cash and Carp method. Appl Math Mech. 2019;40:861–76.
[80] Reddy NB, Poornima T, Sreenivasulu P. Influence of variable thermal conductivity on MHD boundary layer slip flow of ethylene-glycol based Cu nanofluids over a stretching sheet with convective boundary condition. Int J Eng Math. 2014;2014:905158.
[81] Maxwell J. A Treatise on electricity and magnetism. second edition. Oxford, UK: Clarendon Press; 1881.

[82] Ali HM. Hybrid nanofluids for convection heat transfer. Elsevier, USA: Academic Press; 2020.
[83] Xu X, Chen S. Cattaneo–Christov heat flux model for heat transfer of Marangoni boundary layer flow in a copper-water nanofluid. Heat Transfer-Asian Res. 2017;46:1281–93.
[84] Ghadikolaei SS, Hosseinzadeh K, Ganji DD. MHD radiative boundary layer analysis of micropolar dusty fluid with graphene oxide (Go)-engine oil nanoparticles in a porous medium over a stretching sheet with Joule heating effect. Powder Technol. 2013;338:425–37.
[85] Iqbal Z, Azhar E, Maraj EN. Performance of nano-powders SiO_2 and SiC in the flow of engine oil over a rotating disk influenced by thermal jump conditions. Phys A. 2021;565:125570.
[86] Jamshed W. Numerical investigation of MHD impact on Maxwell nanofluid. Int Commun Heat Mass Transf. 2021;120:104973.
[87] Brewster MQ. Thermal radiative transfer and features. Hoboken, New Jersey, U.S.: John Wiley and Sons; 1992.
[88] Qureshi IH, Nawaz M, Rana S, Hayat T. Galerkin finite element study on the effects of variable thermal conductivity and variable mass diffusion conductance on heat and mass transfer. Commun Theoret Phys. 2018;70:49–59.
[89] Das S, Chakraborty S, Jana RN, Makinde OD. Entropy analysis of unsteady magneto-nanofluid flow past accelerating stretching sheet with convective boundary condition. Appl Math Mech. 2015;36(2):1593–610.
[90] Hussain SM, Jamshed W. A comparative entropy based analysis of tangent hyperbolic hybrid nanofluid flow: implementing finite difference method. Int Commun Heat Mass Transf. 2021;129:105671.
[91] Jamshed W, Aziz A. A comparative entropy based analysis of Cu and Fe_3O_4/methanol Powell-Eyring nanofluid in solar thermal collectors subjected to thermal radiation, variable thermal conductivity and impact of different nanoparticles shape. Results Phys. 2018;9:205.